Observation of a threshold behavior in an ultracold endothermic atom-exchange process involving Feshbach molecules

Ya-Xiong Liu, Jue Nan, De-Chao Zhang, Lan Liu, Huan Yang, Jun Rui, Bo Zhao, and Jian-Wei Pan

Hefei National Laboratory for Physical Sciences at Microscale and Department of Modern Physics, University of Science and Technology of China, Hefei, Anhui 230026, China

and Shanghai Branch, CAS Center for Excellence and Synergetic Innovation Center in Quantum Information and Quantum Physics, University of Science and Technology of China, Shanghai 201315, China

(Received 9 June 2019; published 16 September 2019)

We report on the investigation of endothermic and nearly thermoneutral atom-exchange collisions in an ultracold atom-dimer mixture. By developing an indirect preparation method based on a molecular bound-bound transition, we are able to directly observe an endothermic collision with a tunable energy threshold and study the state-to-state collision dynamics. The collision rate coefficients show a striking threshold phenomenon. The influence of the reverse process on the collision dynamics is observed for the endothermic and nearly thermoneutral collisions. We carry out zero-range quantum-mechanical scattering calculations to obtain the collision rate coefficients, and the three-body parameter is determined by comparison with the experiments. The observed endothermic and nearly thermoneutral collisions may be employed to implement quantum simulation of the Kondo effect with ultracold molecules.

DOI: 10.1103/PhysRevA.100.032706

Chemical reactions and inelastic collisions at ultracold temperatures provide an ideal platform to study chemical reactivity at the fundamental level [1–4]. Recently, significant progress has been achieved in studying ultracold chemistry or inelastic collisions with ultracold molecules [5–17]. In particular, the molecule-molecule reaction [9–11] and the atom-exchange process involving weakly bound Feshbach molecules [12–14,18] have been observed at temperatures below 1 μK. The atom-exchange reaction involving weakly bound Feshbach molecules offer a unique candidate to demonstrate the full controllability of ultracold chemistry. The reaction can be tuned to be exothermic, endothermic, or thermoneutral by simply varying the magnetic field. The collision product can be detected, and the collision dynamics can be studied in a state-to-state manner.

Despite the easy tunability of the energetics, the state-to-state dynamics of the atom-exchange process is only studied in the exothermic regime, and the direct observation of the state-to-state endothermic collisions and the measurement of the collision rate remain elusive. In Ref. [12], the overall loss rate of the molecule collision partner is measured, and the atom product is observed in the exothermic regime. It shows a threshold when entering from the endothermic regime to the exothermic regime. However, the measured overall loss rate includes the contribution from both the exchange process and the vibrational relaxation into deeply bound states. The theoretical calculation therein shows that, in the exothermic regime, the exchange process is the dominant factor in the overall losses of the molecules, whereas in the endothermic regime, the collision rate decreases quickly with the increasing of the collision energy threshold, and the dominant loss mechanism is actually the vibrational relaxation. In Ref. [14], the state-to-state rate coefficient can only be measured in the exothermic regime with high released energy. The study of endothermic collision has to satisfy three conditions, i.e., the threshold can be precisely measured and controlled, the collision partners can be efficiently prepared, and the time evolution of products can be measured. Simultaneously meeting these requirements for an endothermic collision is quite difficult.

Here, we report on the study of the endothermic and nearly thermoneutral atom-exchange collision in an ultracold atom-dimer mixture. We develop an indirect preparation method by coherently controlling the internal state of the Feshbach molecule. This method allows us to directly observe an endothermic collision with a tunable energy threshold. The state-to-state collision dynamics is measured, and the threshold phenomenon of the rate coefficients is clearly observed. We also find that the reverse process influences the collision dynamics for the endothermic and nearly thermoneutral collisions. The observed rate coefficients are compared with the zero-range quantum-mechanical scattering calculations, and the three-body parameter is determined.

Our experiment starts with approximately 3.0×10^5 ^{23}Na atoms and 1.6×10^5 ^{40}K atoms at about 600 nK in a crossed-beam optical dipole trap. The measured trap frequencies for K are $h \times (250, 237, 79)$ Hz with h being the Planck constant. The Na atoms are prepared in the lowest hyperfine $|f, m_f\rangle_{\mathrm{Na}} = |1, 1\rangle$ state, and the K atoms can be prepared in any hyperfine ground-state $|f, m_f\rangle_{\mathrm{K}} = |9/2, -9/2\rangle \cdots |9/2, 9/2\rangle$.

At a magnetic field near 130 G, the interspecies Feshbach resonance between $|1, 1\rangle$ and $|9/2, -3/2\rangle$ and the Feshbach resonance between $|1, 1\rangle$ and $|9/2, -5/2\rangle$ overlap. The overlapping Feshbach resonances allow studying the atom-exchange collision between weakly bound Feshbach

molecules and atoms [12–14,18]. In our experiment, the collision may be described by $AB + C \rightarrow AC + B$, where A denotes the ^{23}Na atom in the $|1, 1\rangle$ state, and B and C denote ^{40}K atoms in the $|9/2, -5/2\rangle$ and $|9/2, -3/2\rangle$ states, respectively. The AB and AC molecules are the corresponding NaK Feshbach molecules with binding energies $E^{\rm b}_{\rm AB}$ and $E^{\rm b}_{\rm AC}$, respectively. The energy change in the collision is given by $\Delta E = E^{\rm b}_{\rm AB} - E^{\rm b}_{\rm AC}$. The state-to-state collision dynamics can be measured by preparing the collision partners and then monitoring the time evolution of the AB molecule and B product, and the collision rate coefficient is extracted from the time evolution. For detection [14], the AB molecules are dissociated into the $A + |9/2, -7/2\rangle$ state and the B atoms are transferred to the $|9/2, -7/2\rangle$ state by rf pulses, and the AB molecule number and B atom number are determined by measuring the atom number in the $|9/2, -7/2\rangle$ state, respectively.

In the previous works studying ultracold atom-exchange collision with Feshbach molecules, the molecule collision partners are directly formed using magnetic-field association [12,13] or rf association [14]. However, these methods cannot be used to measure the rate coefficient in the endothermic regime either due to the low formation efficiency or due to large background noise caused by the preparation process.

In our system, the primary experimental challenge is to efficiently prepare the $AB + C$ mixture at the magnetic fields where endothermic collisions with small ΔE may occur. For the exothermic collisions with large and negative ΔE's, the collision partners can be prepared by rf association [14,19] of the AB molecule from an $A + C$ mixture. However, this preparation method is not applicable for small $|\Delta E|$ because in this regime the scattering lengths $a_{\rm AB}$ and $a_{\rm AC}$ in the two scattering channels are close to each other. This results in a rather low association efficiency since the bound-free Franck-Condon factor $F_{\rm bf} \propto (1 - a_{\rm AC}/a_{\rm AB})^2$ is largely suppressed [20].

To circumvent this problem, we develop an indirect preparation method based on the molecular bound-bound transition. Instead of directly forming the AB molecules, we first associate the AC molecules from the $A + |9/2, -1/2\rangle$ mixture and then transfer the weakly bound molecules from the AC to the AB state by an rf π pulse. A subsequent rf π pulse transferring the free K atoms from the $|9/2, -1/2\rangle$ state to the C state then prepares the desired collision partners. The idea behind this method is that, for a small $|\Delta E|$, the suppression of the bound-free Franck-Condon factor is accompanied by an enhancement of the bound-bound Franck-Condon factor [20] $F_{\rm bb} \propto 4a_{\rm AC}a_{\rm AB}/(a_{\rm AC} + a_{\rm AB})^2$. Therefore, although it is difficult to form the AB molecule from the $A + C$ scattering state, it does allow us to create the AB molecule from the AC bound state. The indirect preparation method is more difficult than the preparation methods in previous works since it requires not only the association of the molecule, but also the precise and careful control of the internal states of the Feshbach molecule.

The Feshbach resonance between the A and the C atoms tends to be closed-channel dominated, and thus, the AC molecules can only be efficiently associated when close to the resonance. In our experiment, we employ the Raman photoassociation method, which can efficiently form the AC molecules in a small magnetic-field window between 130.02 and 130.38 G. To manipulate the molecular internal states, the bound-bound rf spectrum and Rabi oscillation are measured as shown in Fig. 1. The difference between the bound-bound transition frequency and the free-free transition frequency precisely determines the energy change $\Delta E = h(\nu_{\rm AC\rightarrow AB} - \nu_{C\rightarrow B})$ of the collision, which is in the range of $h \times (-82, 32)$ kHz. The measured ΔE as a function of the magnetic field is shown in Fig. 2. The polynomial fit yields $\Delta E = 0$ at $B_{\rm tn} = 130.249(2)$ G, which agrees well with the value of 130.24(1) G determined from the intersection point of the binding energy curves. Thanks to the enhanced bound-bound Franck-Condon factor, the bound-bound transition has an efficiency of better than 95%, and approximately 2×10^4 AB molecules are formed. After preparing the collision partners, the time evolutions of the AB molecule and the b atom are recorded.

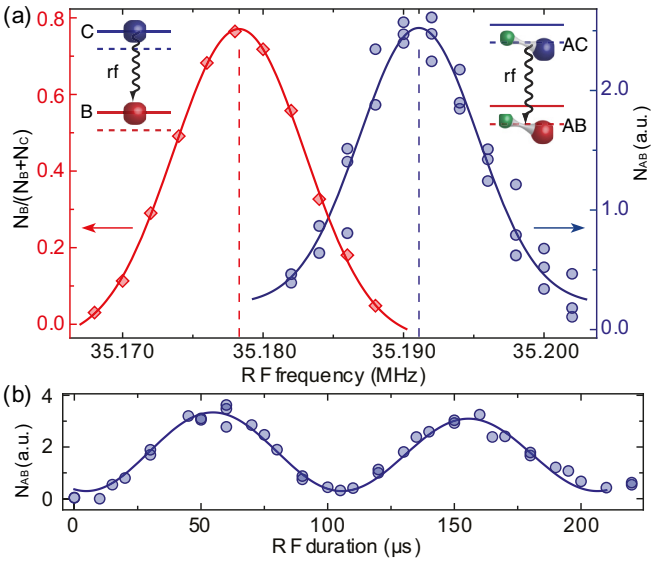

FIG. 1. Molecular bound-bound rf spectrum and Rabi oscillation. (a) The measured atomic transition spectrum (red diamonds) and molecular bound-bound spectrum (blue circles) at 130.29 G. For the atomic spectrum, the fraction of the B atoms is recorded. For the molecular spectrum, the number of molecules transferred into the AB state is recorded by imaging the dissociated K atoms in the $|9/2, -7/2\rangle$ state. The data points are fitted with Gaussian functions. (b) The measured bound-bound Rabi oscillation between the AB and AC molecule states at 130.26 G. The bound-bound Rabi frequency is fitted to be $2\pi \times 9.9(1)$ kHz.

The collision dynamics are shown in Fig. 3. For magnetic fields larger than $B_{\rm tn}$, the collision is endothermic with $\Delta E > 0$. At 130.25 G, the observed collision is nearly thermoneutral with the measured energy change $\Delta E = h \times 1.1(2)$ kHz. The achievable minimal energy change is limited by the resolution and uncertainty of the magnetic field. With increasing magnetic field, the collision threshold increases, and the maximum number of the B products decreases quickly. Using the indirect preparation method, the endothermic collision is clearly observed up to 130.38 G with a threshold of 32 kHz.

We analyze the data by fitting the time evolution of the AB molecule and B atom numbers using exponentials. As shown

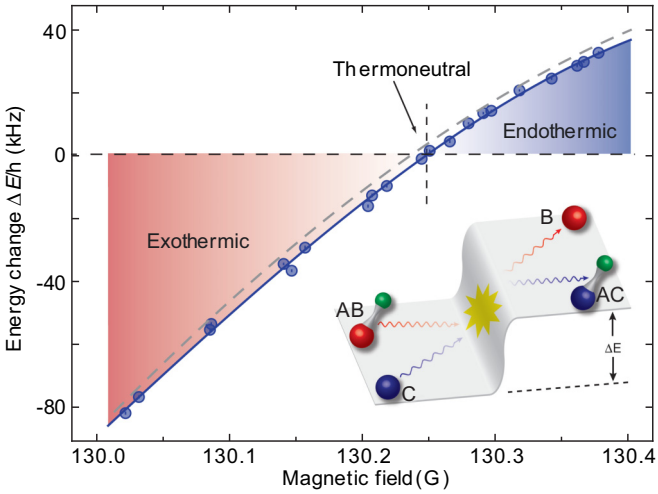

FIG. 2. The collision energy changes versus magnetic field. The measured energy change ΔE for the atom-exchange collision $AB + C \rightarrow AC + B$ as a function of the magnetic field. The energy change is precisely determined by measuring the molecular bound-bound transition frequency and the free atom-atom transition frequency using rf spectroscopy. The blue solid line is a polynomial fit to the data points. The vertical dashed line marks the magnetic-field $B_{\rm tn} = 130.249(2)$ G at which the collision is thermoneutral with zero energy change. For $B < B_{\rm tn}$, the collision is exothermic, and for $B > B_{\rm tn}$, the collision is endothermic. As a comparison, the gray dashed line shows the energy change obtained from the difference between the two binding energy curves. Error bars inside the circles represent ± 1 s.d. where s.d. represents standard deviation.

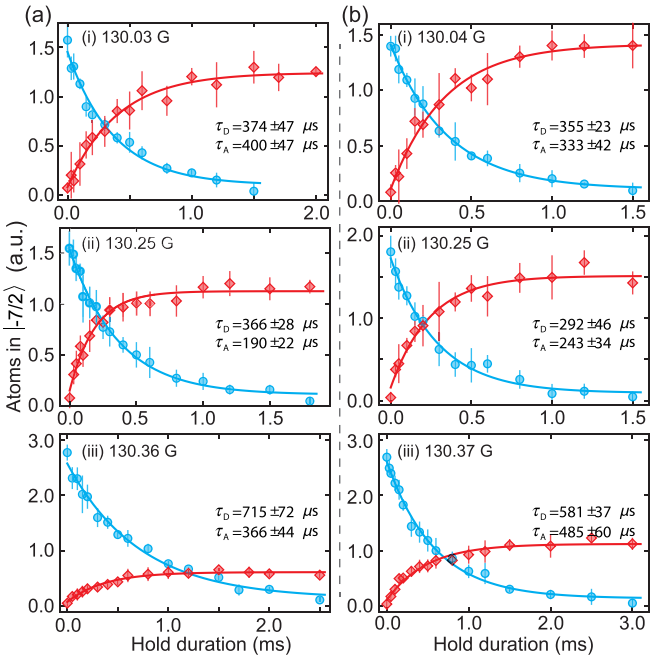

FIG. 3. The collision dynamics. (a) The decay of the AB reactant (blue circles) and the increase in the B product (red diamonds) as a function of the hold time for (i) the exothermic collision at $B = 130.03$ G with $\Delta E = -76.7(3)$ kHz, (ii) the nearly thermoneutral collision at $B = 130.25$ G with $\Delta E = 1.1(2)$ kHz, and (iii) the endothermic collision at $B = 130.36$ G with $\Delta E = 28.0(2)$ kHz. The blue and red solid lines are exponential fitting curves with $1/e$ as time constants $\tau_{\rm AB}$ and τ_B, respectively. For the exothermic collision, $\tau_{\rm AB}$ and τ_B agree with each other within mutual uncertainties, whereas for the endothermic and nearly thermoneutral collisions, $\tau_{\rm AB}$ and τ_B are not consistent. (b) The time evolution of the AB reactant (blue circles) and the B product (red diamonds) after continuously removing the AC product in the collision process. The two time constants $\tau_{\rm AB}$ and τ_B are consistent with each other within the mutual uncertainties also for the endothermic and nearly thermoneutral collisions, and the increased numbers of the B products are larger. Error bars represent ± 1 s.d.

in Fig. 3(a), we find that for the exothermic collisions, the two $1/e$ time constants $\tau_{\rm AB}$ and τ_B agree with each other within mutual uncertainties, whereas for the endothermic and nearly thermoneutral collisions, the two time constants are different from each other. We attribute this discrepancy to the influence of the reverse process $AC + B \rightarrow AB + C$, i.e., the collision is reversible.

To demonstrate that this discrepancy is caused by the reverse process, we continuously remove the AC molecule products from the mixture by dissociating them into the $A + |9/2, -1/2\rangle$ state. To do so, we first remove the A atoms after the AB molecules have been prepared. Then during the collision process, we use the Raman light to continuously dissociate the AC molecules into the $A + |9/2, -1/2\rangle$ state. This procedure suppresses the reverse process and makes the collision irreversible. In this way, we find $\tau_{\rm AB}$ and τ_B agree with each other within mutual uncertainties also for the endothermic and nearly thermoneutral collisions as shown in Fig. 3(b).

We now estimate the collision rate coefficient β_r from the measured time evolutions. Taking the reverse process into account, the time evolution of the number of B products may be described by

$$\dot{N}_B = \beta_r \bar{n}_C N_{\rm AB} - k_{\rm re} N_{\rm AC} N_B, \tag{1}$$

where the first and second terms on the right side of Eq. (1) account for the forward and reverse processes, respectively. By continuously removing the AC products, the second term can be safely neglected. The mean density of the C atoms is approximated by $\bar{n}_C = \alpha N_C$ with $\alpha = [(m_{\rm K}\bar{\omega}^2)/(4\pi k_B T)]^{3/2}$, where $\bar{\omega}$ and T are the geometric mean of the trap frequencies and the temperature, respectively. We have assumed $\bar{n}_C$ to be a constant as the number of the AB molecules is about one order of magnitude smaller than the number of the C atoms. The reverse process complicates the collision dynamics, but the rate coefficient may still be extracted using the simple equation,

$$\beta_r = \frac{\dot{N}_B(0)}{\bar{n}_C N_{\rm AB}(0)}, \tag{2}$$

where $N_{\rm AB}(0)$ is the initial number of the AB molecules and $\dot{N}_B(0)$ is the initial derivative of the time evolution of the B atoms. Equation (2) is also applicable to the reversible process since we start from the $AB + C$ mixture and, thus, at $t = 0$ the products $N_{\rm AC}$ and N_B are both negligible. We assume that $N_{\rm AB}(t)$ and $N_B(t)$ can be approximated by exponentials and obtain $\dot{N}_B(0)$ and $N_{\rm AB}(0)$ from exponential fits of the measured data points. As shown in Fig. 4, the rate coefficients

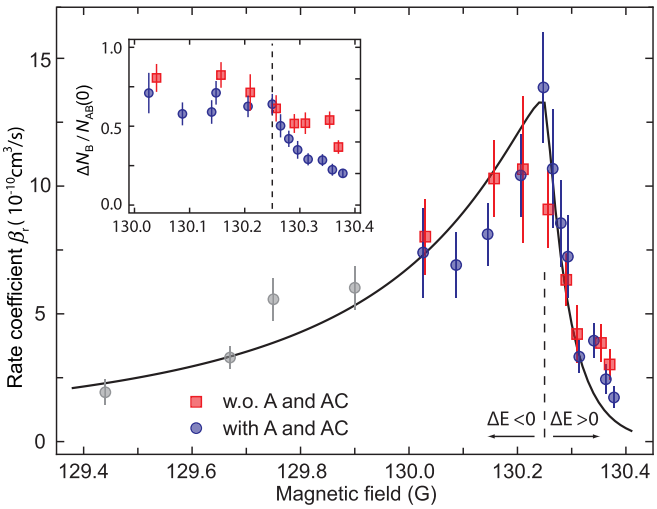

FIG. 4. The behavior of the rate coefficients as a function of the magnetic field. The blue circles and red squares represent the data points measured by using the indirect reactant-preparation method. The red squares are the data points obtained by continuously removing the AC molecules (after eliminating the A atoms) when the reverse processes are significantly suppressed. The gray circles represent the data points obtained from Ref. [14]. The solid line is the numerical result with the fitted three-body parameter $\Lambda = 22.6/a_0$ and the normalization coefficient $C_\beta = 1.4$. The inset shows the ratios between the net increase in the B atom product and the initial AB molecule number where the square points give the branching ratio. Error bars represent ± 1 s.d.

obtained in this way are similar to the results in the case where the reverse process has been suppressed.

For the exothermic collisions, the rate coefficient increases as the magnetic field increases. This may be qualitatively understood from the increase in the overlap between the wave functions of the two weakly bound molecules when the difference between the two scattering lengths decreases [12,18]. For the endothermic collision, the size of the wave functions of the two weakly bound molecules are similar, and the decreasing in the collision rate coefficient versus the magnetic field is dominantly determined by the increase in the collision threshold energy. The rate coefficient shows a strikingly threshold behavior as expected. Besides, the ratio between the increased number of the B products and the initial number of the AB reactants is given in the inset of Fig. 4. The data points after removing the A atoms and the AC molecules directly give the branching ratio of the atom-exchange collision.

To understand the rate coefficient, we perform quantum-mechanical scattering calculations using the zero-range approximation. In our system, the s-wave atom-exchange scattering may be described by the generalized Skorniakov-Ter-Martirosian (STM) equations [21–24]. In the STM equations, the only input parameters are the scattering lengths a_{AB} and a_{AC}, and the unknown three-body parameter Λ, which will be determined by comparing the rate coefficients.

By numerically solving the STM equations, we calculate the rate coefficients with Λ being a fitting parameter. The results are compared with the experiment for the magnetic fields between 129.44 and 130.38 G where the data points for exothermic collisions between 129.44 and 129.991 G are obtained from our previous work [14]. We find that, for a range of values for Λ, the shapes of the theoretical curves and the experimental data points qualitatively agree with each other, whereas the measured rate coefficients are larger than the calculated ones. We attribute this discrepancy to the systematic shifts in our data due to uncertainties in the particle numbers, density calibration, and so on. The contribution of the short-range physics which is not taken into account in the model is also a possible reason. Therefore, we include a normalization factor C_β as the second fitting parameter. As shown in Fig. 4, we find good agreement between the theory and the experiment with the fitting parameters $\Lambda = (22.6 \pm 3.6)/a_0$ and $C_\beta = 1.4 \pm 0.1$, where a_0 is the Bohr radius.

In conclusion, we have studied the endothermic and nearly thermoneutral atom-exchange process in an ultracold atom-dimer mixture. The complete control of an atom-exchange process involving Feshbach molecules has been demonstrated in our paper. The universal character of the interaction allows us to understand the collision from a zero-range approximation. The observed atom-exchange collision can be treated as an indirect spin-exchange interaction between the Feshbach molecule and the K atom, which has been proposed to implement quantum simulation of Kondo effects [25,26]. The direct spin-exchange interaction between B and C may also cause a similar phenomenon. However, in our experiment, the direct spin-exchange scattering length is on the order of $100a_0$. A straightforward estimation gives a direct spin-exchange rate coefficient on the order of 10^{-11} cm^3/s, which is much smaller than the experimental results. Therefore, the spin-exchange interaction is dominantly caused by the indirect atom-exchange process. The spin-exchange interaction in the thermoneutral regime is of crucial importance to the quantum simulation of the Kondo effect since the energy difference between the molecules will polarize the spin like a magnetic field, which suppresses the Kondo effect [25].

We would like to thank P. Zhang, C. Chin, and M. Weidemüller for helpful discussions, and H. Wang, X. Ding, and X.-T. Xu for their important assistance. We acknowledge I. Nosske for carefully reading the paper. This work was supported by the National Key R&D Program of China (under Grant No. 2018YFA0306502), the National Natural Science Foundation of China (under Grants No. 11521063 and No. 11904355), the Chinese Academy of Sciences, the Anhui Initiative in Quantum Information Technologies, and Shanghai Sailing Program (under Grant No. 17YF1420900).

APPENDIX A: FESHBACH RESONANCE

The scattering length near the Feshbach resonance $\tilde{a}(B) = a_{bg}[1 - \Delta B/(B - B_0)]$ has been determined in Ref. [14] by fitting the binding energies of the Feshbach molecules using the universal model. For the Feshbach resonance between A and B, we obtain $a_{bg} = -455a_0$, $B_0 = 138.71$, and $\Delta B = -34.60$ G. For the Feshbach resonance between A and C, we have $a_{bg} = 126a_0$, $B_0 = 130.637$, and $\Delta B = 4.0$ G. The binding energies of the Feshbach molecules are given by

$E_{ij}^{b} = \hbar^2/2\mu_d a_{ij}^2$, where $a_{ij} = \tilde{a}_{ij}(B) - \bar{a}$ with $\bar{a} = 51a_0$ being the mean scattering length. Here a_{AB} and a_{AC} are the input parameters in the STM equations. From the binding energy curves, we obtain $E_{AB}^{b} = E_{AC}^{b}$ at $B = 130.24(1)$ G, which is about 10 mG smaller than $B_{tn} = 130.249(2)$ G which was determined from the direct measurement. Therefore, in the numerical calculations, the magnetic field is shifted by 10 mG to compare with the experiments.

APPENDIX B: RAMAN PHOTOASSOCIATION AND MOLECULAR BOUND-BOUND TRANSITION

In this paper, we employ Raman photoassociation to form AC Feshbach molecules [27]. We use two blue-detuned Raman light fields to couple the $|9/2, -1/2\rangle$ and C states with a single-photon detuning of $\Delta \approx 2\pi \times 251$ GHz with respect to the $D2$ line transition of the ^{40}K atom. The two Raman beams have a frequency difference of approximately $2\pi \times 37$ MHz at the magnetic fields of around 130 G. Thus, they can be simply created by using two acousto-optic modulators with the light field from a single laser. The width of each Raman beam is about 0.8 mm at the position of the atoms, and the power is 30 mW. The Raman Rabi frequency for the $|9/2, -1/2\rangle \rightarrow C$ transition is about $2\pi \times 90$ kHz.

To associate the AC molecules from the $A + |9/2, -1/2\rangle$ mixture, we use a 300-μs Gaussian pulse with a full width at half maximum duration of about 150 μs. Using a Gaussian pulse, the high Fourier side lobes can be efficiently suppressed, and thus, the transfer of free atoms from the $|9/2, -1/2\rangle$ to the C state can be neglected. The Raman light fields have no influence on the active stabilization loop of the magnetic field, and thus, it does not cause a shift of the magnetic field. The efficiency of Raman photoassociation is about 15–20%.

After creating the AC molecules, we determine the molecular bound-bound transition frequency $\nu_{AC\rightarrow AB}$ by measuring the molecule rf spectrum. This is achieved by first transferring the AC molecule to the AB molecule via a rf pulse, and then the AB molecules are detected by dissociating them into the $A + |9/2, -7/2\rangle$ state for imaging. Besides, we also measure the free atomic transition frequency $\nu_{C\rightarrow B}$ by measuring the rf spectrum between the C and the B states. From these measurements, the collision energy change $\Delta E = \nu_{AC\rightarrow AB} - \nu_{C\rightarrow B}$ can be accurately determined, and the results are shown in Fig. 1 in the main text. After determining the bound-bound transition frequency, the Rabi oscillation between the AB and the AC molecule states is measured, and thus, the duration of the π pulse is determined.

APPENDIX C: REMOVE THE REMAINING A ATOMS AND THE AC MOLECULE PRODUCTS

To demonstrate that the discrepancy between the time constants τ_{AB} and τ_B for the endothermic and nearly thermoneutral collision is caused by the reverse process, we remove the AC molecule products continuously during the collision process by dissociating them into the $A + |9/2, -1/2\rangle$ state. However, the remaining A atoms and the residual $|9/2, -1/2\rangle$ atoms due to the imperfection of the π pulse may cause a competition between the dissociation and the association

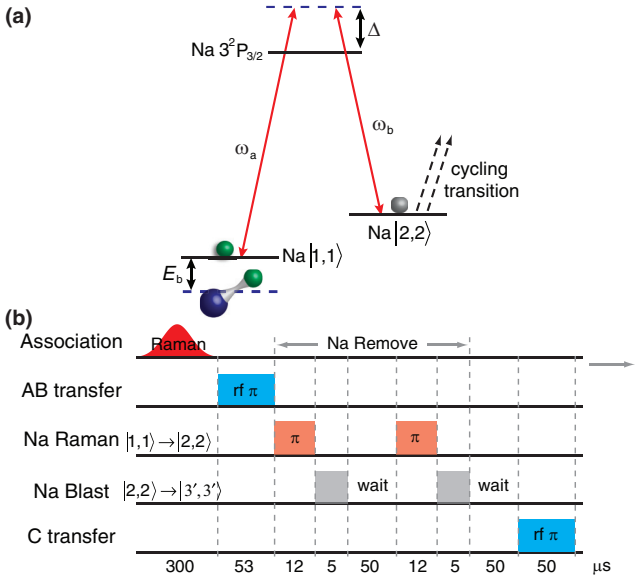

FIG. 5. Removal of the remaining A atoms. (a). The energy levels of the two-photon Raman transition used for transferring the Na atoms from the A to the $|2, 2\rangle$ state. After the Raman transfer, the Na atoms in the $|2, 2\rangle$ state are resonantly blasted out of the optical trap by a light pulse resonant with the cycling transition. (b) The time sequence of the preparation process including the removal of the remaining A atoms.

process. Therefore, we first remove the A atoms after the AB molecules have been prepared. This is achieved as follows. We first transfer Na atoms from the A to the $|2, 2\rangle$ state using a blue-detuned Raman π pulse with a single-photon detuning of $\Delta \approx 2\pi \times 215$ GHz with respect to the $D2$ line of the Na atom and then blast them out of the optical trap by applying a light pulse resonantly coupling the $|2, 2\rangle \rightarrow |3', 3'\rangle$ cycling transition as shown in Fig. 5(a). The Raman fields for Na atoms have a width of about 1.1 mm at the position of the atoms, and each beam has a power of about 50 mW, which yields a Raman-Rabi frequency of $2\pi \times 46$ kHz for the $A \rightarrow |2, 2\rangle$ transition. The Raman-BLAST sequences are applied twice to completely remove the remaining A atoms. The time sequence including the removal of the A atoms is shown in Fig. 5(b). The Raman-BLAST process also causes small loss of the AB molecules. Typically, we still keep 90% of the AB molecules after removing the remaining A atoms.

Then, we can remove the AC molecule products during the collision process by continuously dissociating them into the $A + |9/2, -1/2\rangle$ state. This is achieved by using the Raman light coupling the $|9/2, -1/2\rangle$ and the C states, which is also used to associate the AC molecules. For the dissociation, the two-photon detuning is tuned to be 220–320 kHz above the bound-free transition, and the powers of both beams are reduced to obtain half the peak intensity as was used in the association process. This Raman dissociation light reduces the lifetime of the AC molecules to around 80 μs as is shown in Fig. 6(b), and thus, the AC molecules can be quickly eliminated. We checked that the Raman removing pulse has negligible effects on the C atoms. The Raman removing pulse also affects the lifetime of the AB molecules. However, the AB molecule still has a lifetime of about 2.7 ms under the

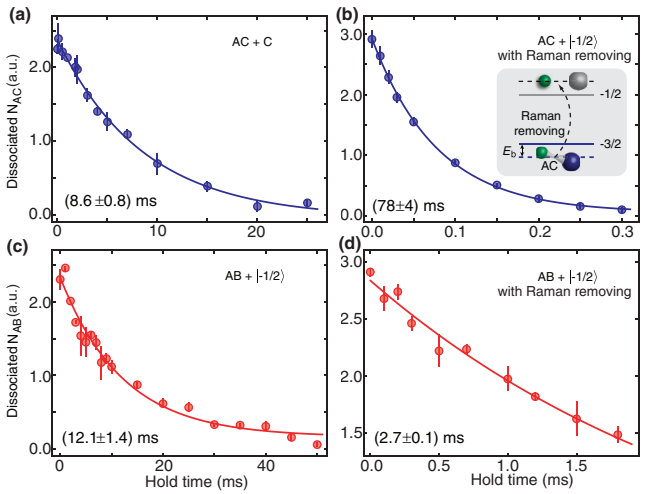

FIG. 6. Lifetime of the molecules under different conditions. The measurements are taken after removing the remaining A atoms at 130.26 G. (a) and (b) The lifetime of the AC molecules without and with the Raman removing fields, respectively. The two-photon frequency is tuned to be about 220 kHz above the bound-free transition frequency. The AC molecules are detected by first transferring them to the AB state and then dissociating them into the $A + |9/2, -7/2\rangle$ state. (c) and (d) The lifetime of the AB molecules without and with the Raman removing fields, respectively. Error bars represent ±1 s.d.

Raman removing fields as is shown in Fig. 6(d), which is long enough for the study of the collision dynamics.

APPENDIX D: COLLISION DYNAMICS

Taking into account the reverse process, the time evolution of the AB molecule and B atom may be described by

$$\dot{N}_{\rm AB} = -\gamma_{\rm AB} N_{\rm AB} + k_{\rm re} N_{\rm AC} N_B, \tag{D1}$$

$$\dot{N}_B = \beta_r \bar{n}_C N_{\rm AB} - k_{\rm re} N_{\rm AC} N_B, \tag{D2}$$

where the first and second terms on the right sides account for the forward and reverse processes, respectively. The time evolution of the AC molecule may be written in a similar form as the AB molecule. Since the time evolution of the AC molecule is difficult to detect, its equation is not shown. Here, the overall loss rate of $N_{\rm AB}$ is $\gamma_{\rm AB} = \beta_A \bar{n}_A + \beta_C \bar{n}_C + \beta_r \bar{n}_C$, with $\bar{n}_A$ and $\bar{n}_C$ as the mean densities of the A and C atoms, respectively. The first term accounts for the loss due to inelastic collisions with the remaining A atoms with β_A as the loss rate coefficient. When the A atoms are removed, this term can be neglected. The other two terms describe the losses due to collisions with the atom C, which include the desired atom-exchange collision with a collision rate coefficient of β_r, and the losses due to collisions in other channels and vibrational relaxations with an overall loss rate of β_C. The collisions between the AB molecules are neglected since the Feshbach molecules are fermionic molecules. We have assumed $\bar{n}_A$ and $\bar{n}_C$ are constants since the number of molecules is about one order of magnitude smaller than that of the atoms. The reverse process is caused by the collisions between the AC molecule and the B atom products with $k_{\rm re}$ as the reverse collision rate.

In our experiment, the time evolutions of $N_{\rm AB}(t)$ and $N_B(t)$ are measured. The rate coefficient is obtained using Eq. (2) in the main text. This is reasonable as we start from the $\mathrm{AB} + C$ mixture, and thus, at $t = 0$, the number of products $N_{\rm AC}$ and N_B can be neglected. The exact form of $N_{\rm AB}(t)$ and $N_B(t)$ are difficult to know. Therefore, we assume they may be approximated by exponentials and use exponentials to fit the data points. The collision rate coefficients are extracted with $N_{\rm AB}(0)$ and $\dot{N}_B(0)$ obtained from the fitting curves. Note that, when the reverse process is suppressed or can be neglected, the analytic solutions of $N_{\rm AB}(t)$ and $N_B(t)$ are exponentials, and thus, collision rate coefficients obtained from Eq. (2) are exact.

The initial molecule number has to be corrected by taking into account the finite rf dissociation rate [14] since the collision is fast. The finite π-pulse transfer efficiency of the K atoms from the B to the $|9/2, -7/2\rangle$ states also needs to be included, which is about 90% with the Na atoms and 95% without the Na atoms. Finally, all uncertainties of the parameters are included to give the uncertainty in the rate coefficients.

APPENDIX E: STM EQUATIONS

The scattering amplitudes satisfy the STM equations,

$$t_{ii}(k, p, E) = \frac{m_A}{\pi \mu_d} \sqrt{\frac{a_{\rm AC}}{a_{\rm AB}}} \int^{\Lambda} dq \frac{q}{2k} K(k, q, E) D_{\rm AC}(q, E) t_{fi}(q, p, E), \tag{E1}$$

$$t_{fi}(k, p, E) = \frac{2\pi\hbar^4}{\mu_d^2 \sqrt{a_{\rm AB} a_{\rm AC}}} \frac{m_A}{2pk} K(k, p, E) + \frac{m_A}{\pi \mu_d} \sqrt{\frac{a_{\rm AB}}{a_{\rm AC}}} \int^{\Lambda} dq \frac{q}{2k} K(k, q, E) D_{\rm AB}(q, E) t_{ii}(q, p, E), \tag{E2}$$

where

$$K(k, p, E) = \ln \frac{2\mu_d E - p^2 - k^2 + 2\mu_d pk/m_A}{2\mu_d E - p^2 - k^2 - 2\mu_d pk/m_A}, \tag{E3}$$

$$D_{\rm jl}(q, E) = \left[-\frac{\hbar}{a_{\rm jl}} + \sqrt{-2\mu_d \left(E - \frac{q^2}{2\mu_{ad}} \right)} \right]^{-1}. \tag{E4}$$

We denote the input channel $\mathrm{AB} + C$ by channel i and the output collision channel $\mathrm{AC} + B$ by channel f, and thus, $t_{ii}(k, p, E)$ is the elastic-scattering amplitude, or in other words, the back-reflection amplitude of scattering into the input channel, $t_{fi}(k, p, E)$ is the reactive scattering amplitude with p and k being the relative momentum of the incoming and outgoing atom-dimer pairs, E is the total energy, $\mu_d = m_A m_B/(m_A + m_B)$ is the reduced mass, and

$\mu_{ad} = m_A(m_A + m_B)/(2m_A + m_B)$ is the reduced mass of the atom and dimer. In the integral equations, the only input parameters are the scattering lengths a_{AB} and a_{AC} and the unknown three-body parameter Λ, which will be determined by comparing the rate coefficients. Since the magnetic-field window in the experiment is narrow, we assume Λ is a constant.

We numerically solve the STM integral equations to calculate the on-shell scattering amplitudes $t_{fi}(k_f, p_i, E)$ with $E = \hbar^2 k_f^2/2\mu_d - E_{AC}^b = \hbar^2 p_i^2/2\mu_d - E_{AB}^b$ using the method introduced in Ref. [23]. The incident relative momentum is calculated for $p_{min} \leqslant p_i \leqslant p_{max}$, where $p_{min} = 0$ for the exothermic collisions, $p_{min} = \sqrt{2\mu_d|\Delta E|}$ for the endothermic collisions, and $p_{max} = \sqrt{2\mu_d E_{AB}^b}$, i.e., we only consider the collisional kinetic energy smaller than the binding energy of the AB molecule. This is a good approximation since in our experiment we have $E_{AB}^b > 4k_BT$. The total collision cross section is given by $\sigma_r(p_i) = (8\pi^3/h^4)\mu_{ad}^2(k_f/p_i)|t_{fi}(k_f, p_i, E)|^2$. The collision rate coefficient is, thus, calculated by $\beta_r = \int v\sigma_r(v)f(v)dv$ where we have $v = p/\mu_{ad}$ and $f(v) = 4\pi v^2[\mu_{ad}/(2\pi k_BT)]^{3/2}\exp[-(\mu_{ad}v^2)/(2k_BT)]$ is the Maxwell-Boltzmann distribution. In the calculation, the temperature is assumed to be 700 nK, and the magnetic field has been shifted 10 mG so that the overlapping magnetic field obtained from the universal binding energy curves is consistent with the direct measurement.

The calculated rate coefficients are compared with the experiment for the magnetic fields between 129.44 and 130.38 G where the data points between 129.44 and 129.91 G are obtained from our previous work. The collision rate at 130.03 G is also measured in our previous work [14]. However, due to the suppression of the bound-free Franck-Condon coefficients, the number of AB molecules that can be formed from the $A + C$ mixture is only about 5000. In comparison, using the indirect method in this paper, 1.5×10^4 AB molecules can be formed. Therefore, at 130.03 G, the collision rate measured in this paper has a much better signal-to-noise ratio and, thus, is used in the fitting. For the magnetic fields larger than 130.03 G, the collision rates can only be measured using the current method.

[1] W. C. Stwalley, Can. J. Chem. **82**, 709 (2004).
[2] R. V. Krems, Phys. Chem. Chem. Phys. **10**, 4079 (2008).
[3] M. T. Bell and T. P. Softley, Mol. Phys. **107**, 99 (2009).
[4] N. Balakrishnan, J. Chem. Phys. **145**, 150901 (2016).
[5] N. Zahzam, T. Vogt, M. Mudrich, D. Comparat, and P. Pillet, Phys. Rev. Lett. **96**, 023202 (2006).
[6] P. Staanum, S. D. Kraft, J. Lange, R. Wester, and M. Weidemüller, Phys. Rev. Lett. **96**, 023201 (2006).
[7] E. R. Hudson, N. B. Gilfoy, S. Kotochigova, J. M. Sage, and D. DeMille, Phys. Rev. Lett. **100**, 203201 (2008).
[8] T. T. Wang, M.-S. Heo, T. M. Rvachov, D. A. Cotta, and W. Ketterle, Phys. Rev. Lett. **110**, 173203 (2013).
[9] S. Ospelkaus, K.-K. Ni, D. Wang, M. H. G. de Miranda, B. Neyenhuis, G. Quéméner, P. S. Julienne, J. L. Bohn, D. S. Jin, and J. Ye, Science **327**, 853 (2010).
[10] K.-K. Ni, S. Ospelkaus, D. Wang, G. Quéméner, B. Neyenhuis, M. H. G. de Miranda, J. L. Bohn, J. Ye, and D. S. Jin, Nature (London) **464**, 1324 (2010).
[11] M. H. G. de Miranda, A. Chotia, B. Neyenhuis, D. Wang, G. Quéméner, S. Ospelkaus, J. L. Bohn, J. Ye, and D. S. Jin, Nat. Phys. **7**, 502 (2011).
[12] S. Knoop, F. Ferlaino, M. Berninger, M. Mark, H.-C. Nägerl, R. Grimm, J. P. D'Incao, and B. D. Esry, Phys. Rev. Lett. **104**, 053201 (2010).
[13] T. Lompe, T. B. Ottenstein, F. Serwane, K. Viering, A. N. Wenz, G. Zürn, and S. Jochim, Phys. Rev. Lett. **105**, 103201 (2010).
[14] J. Rui, H. Yang, L. Liu, D.-C. Zhang, Y.-X. Liu, J. Nan, Y.-A. Chen, B. Zhao, and J.-W. Pan, Nat. Phys. **13**, 699 (2017).
[15] B. Drews, M. Deiß, K. Jachymski, Z. Idziaszek, and J. H. Denschlag, Nat. Commun. **8**, 14854 (2017).
[16] L. D. Carr, D. DeMille, R. V. Krems, and J. Ye, New J. Phys. **11**, 055049 (2009).
[17] H. Yang, D.-C. Zhang, L. Liu, Y.-X. Liu, J. Nan, B. Zhao, and J.-W. Pan, Science **363**, 261 (2019).
[18] J. P. D'Incao and B. D. Esry, Phys. Rev. Lett. **103**, 083202 (2009).
[19] C.-H. Wu, J. W. Park, P. Ahmadi, S. Will, and M. W. Zwierlein, Phys. Rev. Lett. **109**, 085301 (2012).
[20] C. Chin and P. S. Julienne, Phys. Rev. A **71**, 012713 (2005).
[21] E. Braaten and H.-W. Hammer, Phys. Rep. **428**, 259 (2006).
[22] E. Braaten, H. W. Hammer, D. Kang, and L. Platter, Phys. Rev. A **81**, 013605 (2010).
[23] K. Helfrich, H.-W. Hammer, and D. S. Petrov, Phys. Rev. A **81**, 042715 (2010).
[24] C. Gao and P. Zhang, Phys. Rev. A **97**, 042701 (2018).
[25] J. Bauer, C. Salomon, and E. Demler, Phys. Rev. Lett. **111**, 215304 (2013).
[26] Y. Nishida, Phys. Rev. Lett. **111**, 135301 (2013).
[27] Z. Fu *et al.*, Nat. Phys. **10**, 110 (2014).